

Coplanar Waveguide-fed Ultra-wideband Planar Antenna with WLAN-band Rejection

A. Subbarao, S. Raghavan

*Department of Electronics and Communication Engineering
National Institute of Technology, Tiruchirappalil, India
E-mails: subbarao_ka@yahoo.com, raghavan@nitt.edu*

Abstract— A compact coplanar waveguide (CPW)-fed ultra-wideband (UWB) antenna is proposed with band-notched characteristic. The antenna has compact size of 29 x 31 mm². A novel wide polygon-slot is inserted on the antenna to obtain good impedance matching and wide bandwidth. A tapered radiating patch is placed inside the polygon-slot. An embedded C-slot in the radiating patch avoids potential interference from WLAN band. The antenna is fabricated and measured. The measured results confirm that the antenna has operating frequency band of 3.1-10.6 GHz with notched band of 5.1-5.9 GHz. The antenna has stable radiation patterns and consistent gain over operating band. The time domain group delay of antenna is within 1 ns except in notched band, which indicates good linear phase response. The results indicate that the antenna is good for portable UWB systems.

Index Terms— band rejection, group delay, impedance matching, slot, UWB.

I. INTRODUCTION

Since Federal Communication Commission (FCC) released a frequency band of 3.1-10.6 GHz for commercial UWB applications, UWB technology has gained attention in both industry and academia. UWB systems have various merits such as lower power consumption and high data transmission rate. UWB antenna is one of the key elements in UWB systems. Hence, design of UWB antenna has gained attraction in wireless field. Since small antennas are required for portable systems, miniaturization of UWB antenna has become important research topic. Planar slot antennas [1]-[3] have become popular among recently proposed antennas due to small size, wide bandwidth and ease of integration with RF front ends.

Several narrow band communication systems such as IEEE 802.11a wireless local area network (WLAN) bands (5.15-5.35 GHz and 5.725-5.825 GHz) in USA and high performance radio local area network/2 (HIPERLAN/2) bands (5.15-5.35 GHz and 5.470-5.725 GHz) in Europe, exist in ultra-wide bandwidth. Hence, potential interference from these bands should be avoided for good performance of UWB antenna. UWB filters [4], [5] have been designed to suppress the undesired bands. However, use of filter increases complexity of overall UWB system. Hence, it is required to design UWB antenna with band-notched characteristics. Various UWB antennas with band-notched techniques

have been proposed in literature such as cutting a π -slot [6], [7], arc-slot [8] in patch, embedding a tuning stub in slot [9], [10], inserting a slit in patch [11] and placing parasitic elements near feed [12], [13]. However, the time domain analysis of UWB antenna is not analyzed with mathematical expressions. The CPW feed is popular because it has wider bandwidth, lesser dispersion and lower radiation loss than microstrip line.

In this paper, a compact UWB slot antenna is presented with band-rejection characteristic. By inserting a C-slot in the radiating patch, the interfering signals from WLAN band are avoided. The geometry of antenna is presented in section II with band-notched design. The parametric study of antenna is analyzed in section III. The measured radiation patterns and gain are discussed in section IV. The time domain analysis of antenna is analyzed in section V. The time domain group delay of antenna is with in 1ns except in notched band. The transient response of antenna is explained with mathematical expressions. Section VI concludes the paper.

II. ANTENNA GEOMETRY AND BAND-NOTCHED DESIGN

The antenna is fabricated on FR4 substrate with dielectric permittivity $\epsilon_r = 4.4$, loss tangent $\tan\delta = 0.02$ and thickness $h = 0.8$ mm. The antenna has compact size of 29×31 mm². The antenna is fed by 50 Ω CPW line. The CPW feed is terminated with subminiature version A (SMA) connector. A single metallic layer and small size make the antenna to integrate with RF front ends easily. A novel polygon-slot was chosen to obtain wide bandwidth and good impedance matching over the bandwidth. Hence the parameters W_3 , L_3 and L_4 are optimized to obtain good impedance matching over UWB. A radiating tapered patch is placed inside polygon-slot as shown in Fig. 1.

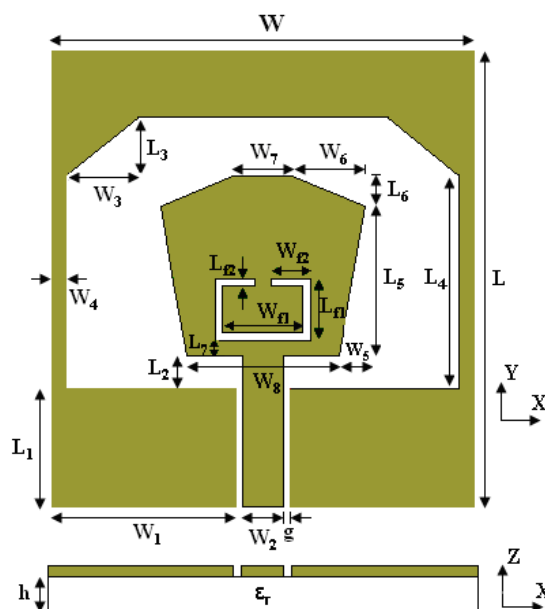


Fig. 1. Geometry of the proposed UWB antenna.

A 'C' shaped slot is inserted in the radiating patch of antenna to avoid interference from WLAN and HIPERLAN/2 bands as shown in Fig. 1. Since the slot is considered as half wave resonator, guided wavelength is used to obtain total length of C-slot. When the length of the C-slot is about half

of guided wavelength λ_g , the slot resonates at notch frequency f_0 and behaves as short circuit in parallel to input impedance of the antenna. Hence, the antenna does not work in the frequencies around f_0 and it avoids the potential interference from WLAN band from 5.1 GHz to 5.9 GHz. Let, the total length of C-slot [14] is denoted by L_{slot} and it is obtained by

$$L_{slot} = \frac{\lambda_g}{2} = \frac{c}{2f_0 \sqrt{\frac{\epsilon_r + 1}{2}}} \quad (1)$$

where λ_g is guided wavelength corresponding to notch frequency f_0 , c is velocity of light in free-space and ϵ_r is dielectric permittivity of FR4 substrate. Initially, C-slot is designed theoretically to resonate at notch frequency $f_0 = 5.5$ GHz to obtain total length of C-slot according to equation 1. In practice, the notch frequency $f_0 = 5.5$ GHz is obtained when the total length of C-slot is $L_{slot} = W_{f1} + 2W_{f2} + 2L_{f1} + 2L_{f2}$ as shown in Fig. 1 in the design of antenna structure with IE3D electromagnetic solver. Hence, the length L_{slot} is practically equal to $0.6\lambda_g$ where $\lambda_g = \lambda_0 / \sqrt{\epsilon_{eff}}$ and $\epsilon_{eff} = (\epsilon_r + 1) / 2$. Here, λ_0 is wavelength corresponding to the notch frequency $f_0 = 5.5$ GHz, ϵ_{eff} is effective dielectric permittivity of dielectric substrate and ϵ_r is dielectric permittivity of the substrate. The proposed fabricated antenna with the total length of C-slot L_{slot} confirms the measured notched frequency 5.5 GHz as shown in Fig. 2.

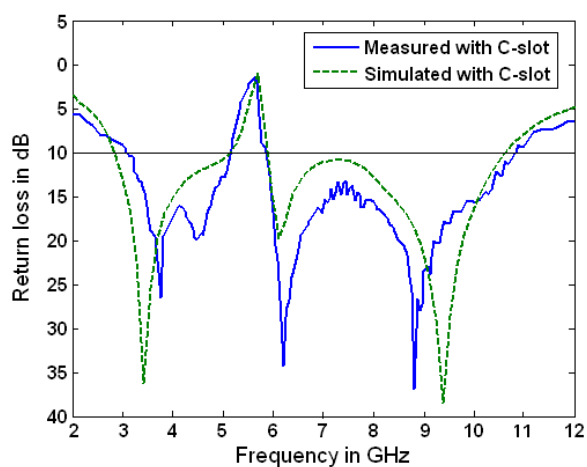


Fig. 2. Simulated and measured return losses of proposed antenna.

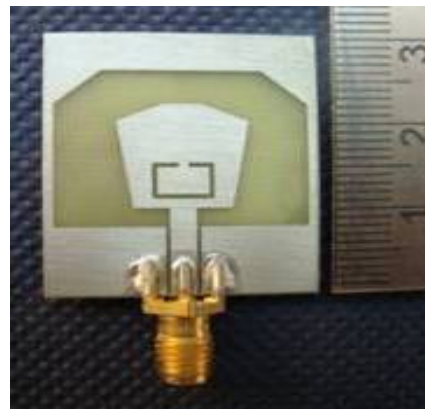


Fig. 3. Photograph of the fabricated antenna.

The antenna parameters are optimized based of method of moments based IE3d electromagnetic optimizer. The optimized parameters of the proposed antenna are $W = 29$ mm, $W_1 = 12.65$ mm, $W_2 = 2.8$ mm, $W_3 = 5$ mm, $W_4 = 1$ mm, $W_5 = 1.75$ mm, $W_6 = 5$ mm, $W_7 = 4$ mm, $W_8 = 10.5$ mm, $W_{f1} = 5.5$ mm, $W_{f2} = 2.75$ mm, $L = 31$ mm, $L_1 = 8$ mm, $L_2 = 2.2$ mm, $L_3 = 4$ mm, $L_4 = 4.5$ mm, $L_5 = 10.25$ mm, $L_6 = 2$ mm, $L_7 = 1.1$ mm, $L_{f1} = 4.2$ mm, $L_{f2} = 0.5$ mm, $g = 0.45$ mm. The fabricated antenna is measured with Agilent E8362B network analyzer. The simulated and measured return loss curves of proposed antenna are shown in Fig. 2. Good agreement is found between measured and simulated

return loss curves. The difference between them is mainly due to effect of soldering at SMA connector and slight variation of dielectric permittivity, dissipation factor at high frequencies. The antenna has impedance bandwidth of 3.1-10.6 GHz with a notched band from 5.1 GHz to 5.9 GHz. The Fig. 2 shows that the measured UWB antenna has three resonating frequencies 3.8 GHz, 6.2 GHz and 8.8 GHz. The photograph of fabricated antenna is shown in Fig. 3.

III. PARAMETRIC ANALYSIS

The effect of few sensitive parameters on the performance of antenna has been studied. The analysis is done by changing one parameter, keeping all other parameters constant. IE3d simulator is used in this analysis.

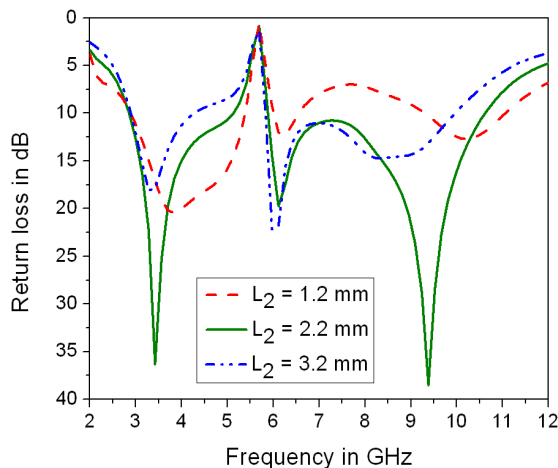


Fig. 4. Simulated return loss curves of antenna for different intrusion depths L_2 .

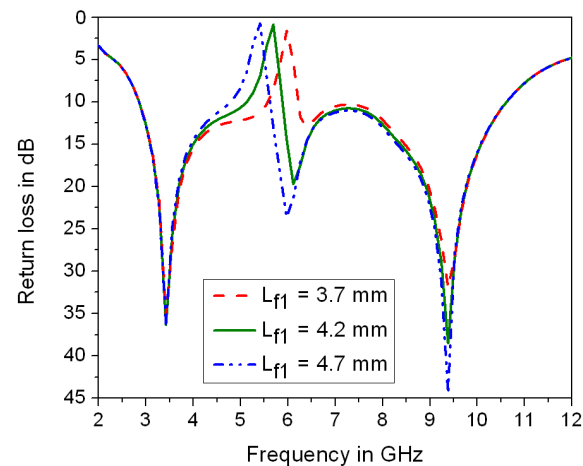


Fig. 5. Simulated return loss curves of antenna for different intrusion depths L_{f1} of C-slot.

A. Effect of intrusion depth L_2

The intrusion depth L_2 affects impedance matching and bandwidth of antenna as shown in Fig. 4. It causes more current distribution at bottom part of patch and top edge of ground plane as shown in Fig. 9(a) when L_2 is 2.2 mm. This parameter produces impedance mismatching when L_2 changes from 2.2 mm. Hence, L_2 is optimized to obtain better coupling from feed line to patch. The simulation results show that the antenna has poor impedance matching at $L_2 = 1.2$ mm. As L_2 increases, the second resonant frequency changes slightly. The first and third resonant frequencies shift left and impedance bandwidth also varies. The antenna covers entire ultra-wide bandwidth at optimum value $L_2 = 2.2$ mm. Table I shows the effect of intrusion depth on simulated lower cut-off frequency f_{lower} , upper cut-off frequency f_{upper} and resonating frequencies. It is clear that f_{upper} decreases and f_{lower} remains constant with increase in L_2 . Hence, the impedance bandwidth decreases. The simulated resonant frequencies also change.

B. Effect of length L_{f1} of C-slot

If slot height L_{f1} increases from 3.7 mm to 4.7 mm, the total length of C-slot increases. The notch frequency f_0 of WLAN changes from 5.9 GHz to 5.4 GHz as shown in Fig. 5. This is mainly due to

the fact that the length of slot L_{slot} is inversely proportional to notch frequency f_0 of slot as mentioned in equation 1. When L_{f1} is 4.2 mm, the C-slot resonates at the notch frequency 5.5 GHz and WLAN band is avoided due to abrupt change in impedance. As L_{f1} varies from 4.2 mm, WLAN and HIPERLAN/2 bands are not fully avoided as shown in Fig. 5. Hence, the notch frequency in WLAN band is controlled by the slot height L_{f1} . Table II shows the effect of length L_{f1} on simulated lower cut-off frequency f_{lower} , upper cut-off frequency f_{upper} , notch frequency f_0 and notch bandwidth. As L_{f1} increases, notch frequency decreases and f_{lower} , f_{upper} remain constant. The frequency range of notched-band changes.

TABLE I. EFFECT OF L_2 ON SIMULATED LOWER CUT-OFF FREQUENCY f_{lower} , UPPER CUT-OFF FREQUENCY f_{upper} AND SIMULATED RESONANT FREQUENCIES

L_2 (mm)	f_{lower} (GHz)	f_{upper} (GHz)	Simulated resonating frequencies (GHz)
1.2	2.88	11.04	3.8, 6.14, 10.25
2.2	2.88	10.61	3.41, 6.10, 9.39
3.2	2.88	9.99	3.29, 5.98, 8.40

TABLE II. EFFECT OF L_{f1} ON SIMULATED LOWER CUT-OFF FREQUENCY f_{lower} , UPPER-CUT OFF FREQUENCY f_{upper} AND SIMULATED NOTCH FREQUENCY f_0 AND SIMULATED NOTCH BANDWIDTH

L_{f1} (mm)	f_{lower} (GHz)	f_{upper} (GHz)	Notch frequency, f_0 (GHz)	Simulated Notch Bandwidth (GHz)
3.7	2.88	10.61	5.9	5.57-6.22
4.2	2.88	10.61	5.5	5.12-5.88
4.7	2.88	10.61	5.4	4.78-5.62

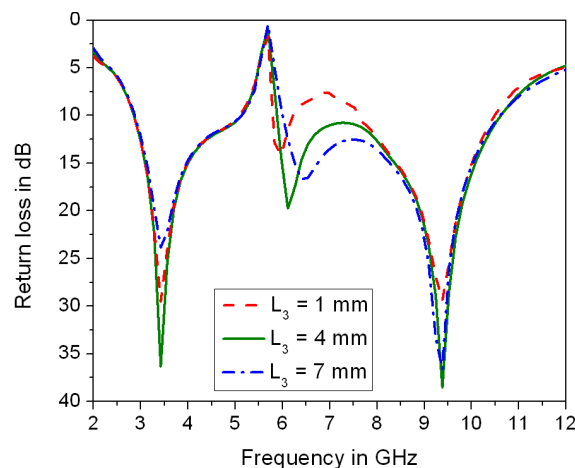


Fig. 6. Simulated return loss curves of antenna for different heights L_3 .

C. Effect of height L_3 at upper part of ground plane

The influence of height L_3 on resonant frequencies and bandwidth of antenna is observed. As L_3 decreases from 7 mm to 1 mm, the value of second resonant frequency decreases as shown in Fig. 6.

The impedance matching at second resonant frequency deteriorates. The impedance matching is better at optimized value of $L_3 = 4$ mm. Hence, this parameter plays important role in improving impedance match around second resonant frequency.

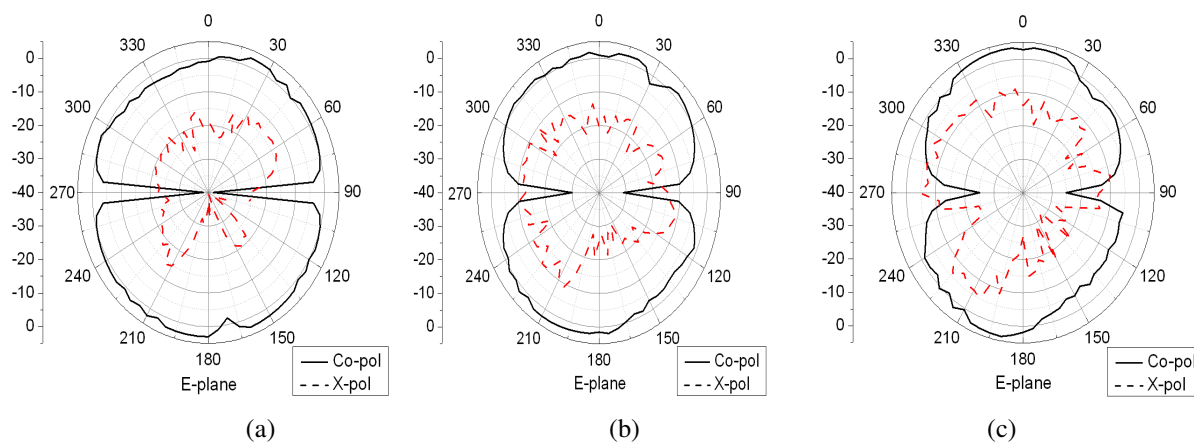


Fig. 7. Measured radiation patterns of proposed antenna in E-plane at (a) 3.8 GHz (b) 6.2 GHz (c) 8.8 GHz.

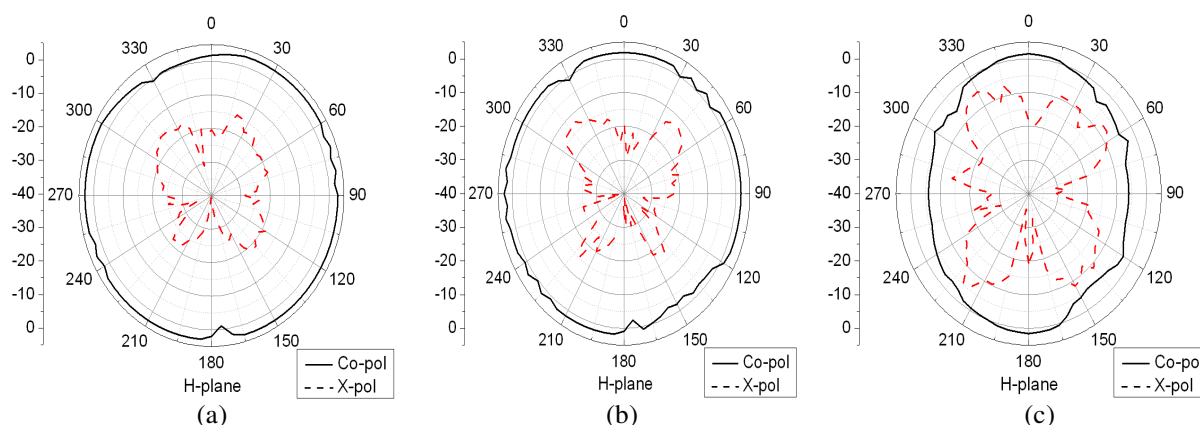


Fig. 8. Measured radiation patterns of proposed antenna in H-plane at (a) 3.8 GHz (b) 6.2 GHz (c) 8.8 GHz.

IV. RADIATION PATTERN AND CURRENT DISTRIBUTION

The radiation patterns are measured using anechoic chamber. Figs. 7, 8 present co-polarization, cross polarization radiation patterns of the band-notched antenna in both E and H planes at measured resonant frequencies 3.8 GHz, 6.2 GHz, 8.8 GHz. The antenna has figure of eight shaped radiation patterns in E-plane which indicate that the antenna has bidirectional radiation patterns in this plane. The antenna has stable omni directional radiation patterns in H plane except at 8.8 GHz. The radiation pattern is slightly deviated from omni directional pattern in H-plane at 8.8 GHz. This is mainly due to presence of higher order modes at higher frequencies.

The radiation pattern relates to current distribution over entire operating band. Fig. 9 represents the simulated current distribution at resonant frequencies 3.8 GHz, 5.5 GHz, 6.2 GHz and 8.8 GHz. At 3.8 GHz, the surface current distribution is mainly on feed line, lower portion of patch, outer edge of patch and edges of the ground plane as shown in Fig. 9(a). Hence, these regions contribute more to radiation. At notch frequency of 5.5 GHz, strong surface current distribution concentrates at the edges

of C-slot and flows back to feeding cable as shown in Fig. 9(b). Hence, the high impedance at the slot changes to nearly zero impedance at feed cable. Hence, there is abrupt change in impedance matching and this impedance mismatch rejects WLAN band. At 6.2 GHz, the X-directed current distribution produces cross polarization in H-plane.

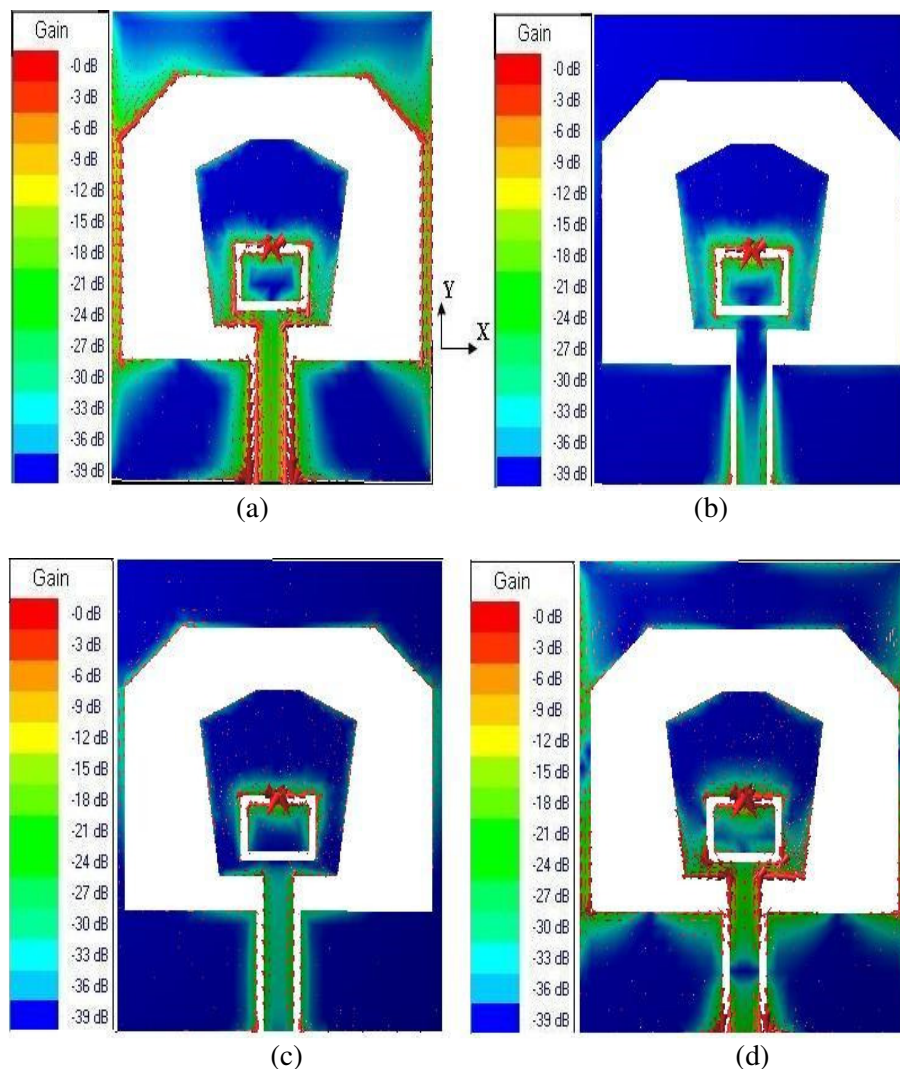


Fig. 9. Surface current distribution on antenna at (a) 3.8 GHz (b) 5.5 GHz (c) 6.2 GHz (d) 8.8 GHz.

At 8.8 GHz, the cross polarization increases as shown in Fig. 8(c) because of presence of more X-directed current components at lower part of patch and top edge of ground plane as observed in Fig. 9(d). Fig. 10 represents measured gain of antenna against frequency. The antenna has consistent gain that changes from 2.1 dBi to 5.8 dBi in UWB except in notched band. There is sharp decrease of gain around 5.5 GHz in notched band. This confirms rejection of WLAN and HIPERLAN/2 bands.

V. TIME DOMAIN ANALYSIS

Since group delay presents phase linearity in far-field, it is an important parameter in time domain. Hence, group delay measurement is obtained by keeping two identical antennas at a distance of 20 cm at far-field in face to face orientation. Fig. 11 shows the time domain group delay response. The graph indicates that the group delay variation is within 1 nano second except in notched band. Hence, the

antenna has linear phase response and good pulse handling capability.

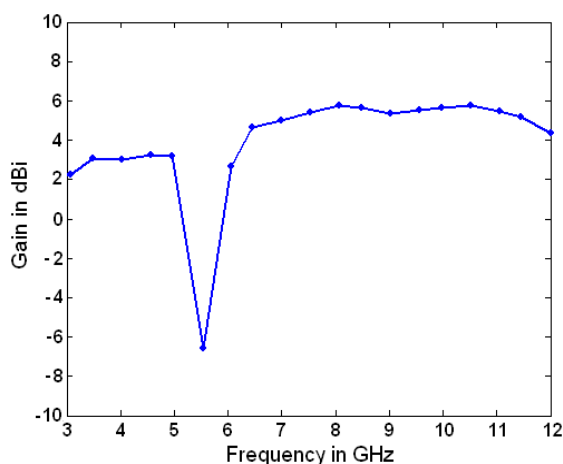


Fig. 10. Measured gain of proposed antenna.

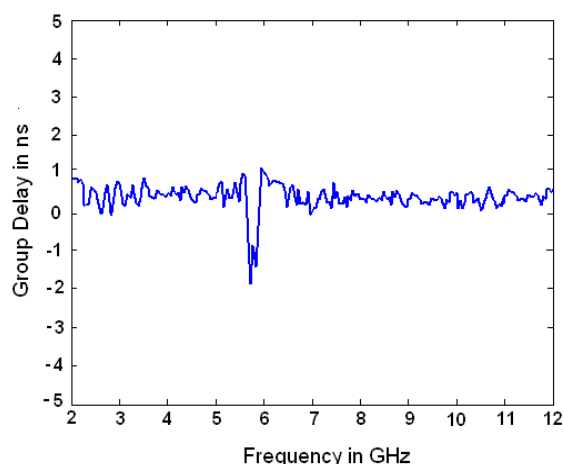


Fig. 11. Measured group delay of proposed antenna.

Since UWB antenna transmits pulse signals, the time domain characteristic of UWB antenna is important. The UWB signal propagation is important for communications. To obtain the performance of pulse transmission, two identical antennas are placed in face to face orientation, with a distance of 20 cm between them. The scattering transmission parameter S_{21} of antenna is measured and the transfer function $H(\omega)$ [15] of antenna is obtained from S_{21} as

$$H(\omega) = \sqrt{\frac{2\pi R c S_{21}(\omega) e^{j\omega R/c}}{j\omega}} \quad (2)$$

where c is velocity of light in free-space, R is distance between two identical antennas and ω is angular frequency. The input pulse is Gaussian modulated cosine pulse with amplitude factor $A = 1$, pulse width $T = 200$ picoseconds and centre frequency $f_c = 6.5$ GHz. The time domain input waveform $i(t)$ is represented by

$$i(t) = A \cos(2\pi f_c t) \cdot e^{-t^2/T^2} \quad (3)$$

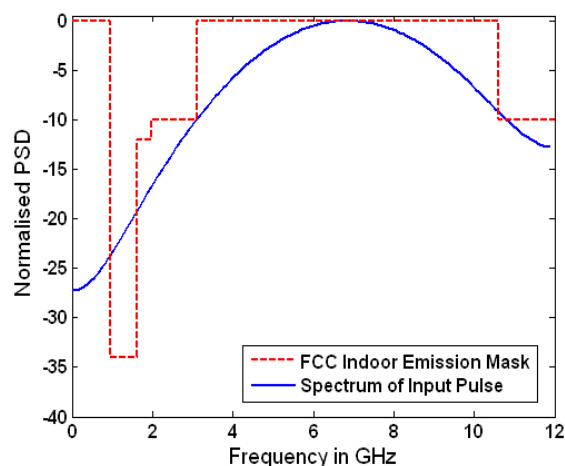


Fig. 12. FCC indoor emission mask and spectrum of input pulse.

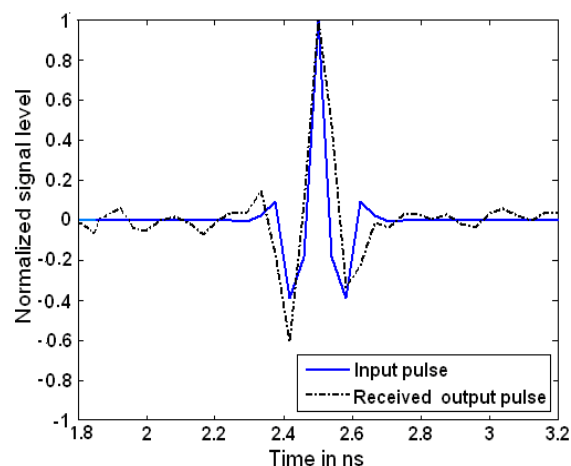


Fig. 13 Comparison of input and output pulses.

The input waveform represented by equation 3 is shifted in time domain by 2.5 ns to avoid negative time and is shown in Fig. 13. The normalized power spectral density (PSD) for indoor emission mask is coded in matlab for input waveform mentioned in equation 3 with a time shift of 2.5 ns and is presented in Fig. 12. The spectrum of input pulse satisfies UWB indoor emission mask specified by FCC from 3.1 GHz to 10.6 GHz as shown in Fig. 12. The output waveform $o(t)$ is computed by the inverse Fourier Transform of product of $H(\omega)$ and spectrum of input signal $I(\omega)$ and is given by

$$o(t) = F^{-1}(H(\omega).I(\omega)) \quad (4)$$

The time domain input and output pulses are displayed in Fig. 13. The slight ringing effect in received pulse is mainly due to transmission characteristics of the system. The received waveform indicates proper transient response for the proposed antenna. Hence, the antenna has good time domain response and it can be used for UWB communications.

VI. CONCLUSION

A compact printed planar UWB slot antenna is presented with band-notched characteristic. The desired notched band of 5.1-5.9 GHz is obtained by inserting C-slot in radiating patch to avoid interference from WLAN and HIPERLAN/2 bands. The antenna operates from 3.1 GHz to 10.6 GHz, except over notched band of 5.1-5.9 GHz. The radiation patterns are stable over UWB. The gain of antenna is almost flat except in the notched band. The group delay of antenna indicates linear phase response and good pulse handling capability. The antenna can be easily integrated with microwave integrated circuits. The antenna is good for portable UWB systems.

ACKNOWLEDGMENT

The authors would like to express sincere gratitude to the scientist, U. S. Pandey, for providing measurement facilities in LRDE lab at Defence Research Development Organisation (DRDO), Bangalore, Govt. of India.

REFERENCES

- [1] A. Mehdipour, K. M. Aghdam, R. F. Dana, and M. R. K. Khatib, "A novel coplanar waveguide-fed antenna for ultrawideband applications," *IEEE Trans. Antennas Propag.*, vol. 56, no. 12, pp. 3857–3862, Dec. 2008.
- [2] N. Farrokh-Heshmat, J. Nourinia, and C. Ghobadi, "Band-notched ultra-wideband printed open-slot antenna using variable on-ground slits," *Electron. Lett.*, vol. 45, no. 21, pp. 1060–1061, Oct. 2009.
- [3] A. Subbarao and S. Raghavan, "A compact UWB Slot antenna with signal rejection in 5-6 GHz band", *Microw. Opt. Technol. Lett.*, vol. 54, no. 5, pp. 1292–1296, May 2012.
- [4] K. Chung, S. Hong, and J. Choi, "Ultrawide-band printed monopole antenna with band-notch filters," *IET Microw. Antennas Propag.*, vol. 1, no. 2, pp. 518–522, Apr. 2007.
- [5] B. Ahmadi and R. Faraji dana, "A miniaturised monopole antenna for ultra-wide band applications with band-notch filter," *IET Microw. Antennas Propag.*, Vol. 3, no. 8, pp. 1224–1231, Feb. 2009.
- [6] K. Song, Y. Z. Yin, and L. Zhang, "A novel monopole antenna with a self-similar slot for wideband applications," *Microw. Opt. Technol. Lett.*, vol. 52, no. 1, pp. 95–97, Jan. 2010.
- [7] Y. L. Zhao, Y. C. Jiao, G. Zhao, L. Zhang, Y. Song, and Z. B. Wong, "Compact planar monopole UWB antenna with band-notched characteristic," *Microw. Opt. Technol. Lett.*, vol. 50, no. 10, pp. 2656–2658, Oct. 2008.
- [8] K. Yin and J. P. Xu, "Compact ultra-wideband antenna with dual bandstop characteristic," *Electron. Lett.*, vol. 44, no. 7, pp. 453–454, Mar. 2008.
- [9] M. Abdollahvand, G. Dadashzadeh, and D. Mostafa, "Compact dual band-notched printed monopole antenna for UWB application," *IEEE Antennas Wireless Propag. Lett.*, vol. 9, pp. 1148–1151, 2010.

- [10] C. Y. Hong, C. W. Ling, I. Y. Tarn, and S. J. Chung, "Design of a planar ultrawideband antenna with a new band-notch structure," *IEEE Trans. Antennas Propag.*, vol. 55, no. 12, pp. 3391–3397, Dec. 2007.
- [11] M. Abdollahvand, G. R. Dadashzadeh, and H. Ebrahimian, "Compact band-rejection printed monopole antenna for UWB application," *IEICE Electron. Exp.*, vol. 8, no. 7, pp. 423–428, Apr. 2011.
- [12] A. M. Abbosh and M. E. Bialkowski, "Design of UWB planar band notched antenna using parasitic elements," *IEEE Trans. Antennas Propag.*, vol. 57, no. 3, pp. 796–799, Mar. 2009.
- [13] L. H. Ye and Q. X. Chu, "Improved band-notched UWB slot antenna," *Electron. Lett.*, vol. 45, no. 25, pp. 1283–1285, Dec. 2009.
- [14] T. Dissanayake and K. P. Esselle, "Prediction of notch frequency of slot loaded printed UWB antennas," *IEEE Trans. Antennas Propag.*, vol. 55, no. 11, pp. 3320–3325, Nov. 2007.
- [15] V. A. Shameena, S. Mridula, A. Pradeep, S. Jacob, A. O. Lindo, and P. Mohanan, "A compact CPW fed slot antenna for ultra wide band applications," *Int. J. Electron. Commun.*, vol. 66, no. 3, pp. 189–194, Mar. 2012.